FIRST INTERANTIONAL CONFERENCE ON FLUID STRUCTURE INTERACTION
FLUID STRUCTURE INTERACTION

CONFERENCE CHAIRMEN

S.K. Chakrabarti
Offshore Structure Analysis Inc., USA

C.A. Brebbia
Wessex Institute of Technology, UK

INTERNATIONAL SCIENTIFIC ADVISORY COMMITTEE

P. Anagnostopoulos	D.B. Ingham	H. Power
S.K. Bhattacharya	A. Jeffrey	M. Rahman
S.K. Chakrabarti	S. Kim	P. Skerget
L. Debnath	A.C. Mendes	J. Skourup
J.P. du Plessis	B. Moodie	P.A. Tyvand
R. Grundmann	W. Perrie	R. Verhoeven
R.C. Gupta	H. Pina	L.C. Wrobel

Organised by:
Wessex Institute of Technology, UK

Fluid Structure Interaction

Edited by

S.K. Chakrabarti
Offshore Structure Analysis Inc., USA

C.A. Brebbia
Wessex Institute of Technology, UK

WITPRESS Southampton, Boston

5 Conclusions

First principle investigations have shown different failure modes for liquid filled containers. These failure modes are depending on mass and velocity of the projectile, and geometry and material of the container. This is a basis for ongoing work to explain also the failure behaviour of concrete containers due to its specific material features.

References

[1] Corbett, G.G., Reid, S.R., Johnson, W. Impact loading of plates and shells by free-flying projectiles: a review. Int. J. Impact Engng. Vol. 18, pp.141-230, 1996.

[2] Leppin, S., Woodward, R.L. Perforation mechanisms in thin titanium alloy targets. Int. J. Impact Engng. Vol. 4, pp. 107-115, 1986.

[3] Neilson, A.J., Howe, W.D., Garton, G.P. Impact resistance of mild steel pipes: An experimental study. Winfrith UKAEA Report AEEW-R 2125, 1987.

[4] Telitchev, I.Y., Schäfer, F.K., Schneider, E.E., Lambert, M. Analysis of the fracture of gas-filled pressure vessels under hypervelocity impact. Int. J. Impact Engng. Vol.23, pp.905-919, 1999.

[5] Woodward, R.L., Cimpoeru, S.J. A study of the perforation of aluminium laminate targets. Int. J. Impact Engng. Vol. 21, pp. 117-131, 1998.

[6] Xiaoqing, Ma, Stronge, W.J. Spherical missile impact and perforation of filled steel tubes. Int. J. Impact Engng. Vol. 3, pp. 1-16, 1985.

[7] Zukas, J.A. In High Velocity Impact Dynamics. pp. 593-714, (Edited by Zukas). John Wiley & Sons 1990.

Nonlinear vibrations of vertical asymmetrically-supported rotors under fluid confinement: theoretical results

M. Moreira[1], H. Pina[2] and J. Antunes[3]
[1]*Politechnic Institute of Setubal, Portugal*
[2]*Technical Institute, Portugal*
[3]*Nuclear Institute, Portugal*

Abstract

This paper is concerned about vertical rotors immersed in fluid annulus of moderate confinement. Such rotors are subjected to the dynamical effects of the fluctuating co-rotating flows.

For high enough spinning velocities, the fluid-elastic forces become significant, and often lead to unstable dynamical regimes. These depend on the fluid gap and density, on the rotor eccentricity and spinning velocity, as well as structural properties.

We developed an improved linear model for rotors under moderate fluid confinement as well as an exact model for the corresponding nonlinear rotordynamics. Recently a symbolic-numerical formulation based on a spectral/Galerkin approach was also developed by the authors. Numerical results showed a quite good agreement between exact solutions and these formulations and experimental validation of the theoretical model has been provided for symmetrically-supported rotors.

Numerical simulations carried over immersed rotor configurations maintained by non-isotropic supports show that the rotor stability is affected by support stiffness-asymmetry.

In this paper, we briefly summarize the theoretical approaches used in the numerical simulations and present an analysis of the linear rotor-dynamics, as a function of the support stiffness-asymmetry and of the rotor eccentricity. Theoretical stability domains are computed from the eigenvalues of the linearized model. Finally, we present time-domain numerical simulations of some stable solutions and nonlinear limit-cycles which stem from linearly-unstable solutions.

1 Introduction

Rotor dynamics under moderate fluid confinement — that is, in equipments with clearance ratios of about $\delta = \frac{H}{R} \approx 0.1$ (where H is the average gap and R the rotor radius) — have been studied since Black [6], Fritz [8] and Hirs [11]. Further relevant work was presented by Ramsden et al. [19] and [20], Childs [7], Nelson

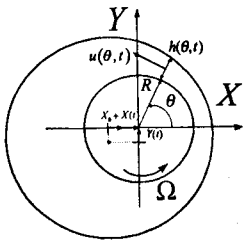

Figure 1: Geometry of the fluid flow

[17] and Nordmann et al. [18]. Thorough analysis using linearized flow equations on the gap-averaged fluctuating quantities were performed by Grunenwald et al. [9], Axisa & Antunes [5], Grunenwald [10] and Antunes et al. [2].

An improved linear model for rotors under moderate fluid confinement (see, Moreira et al. [14]), theoretical formulations for the nonlinear planar motions — with $X(t)$ taking place in one single direction — and for nonlinear orbital motions of rotors — with $X(t)$ and $Y(t)$ taking place in orthogonal directions— were developed and validated by Antunes et al. [3] and Moreira et al. [12] and [13].

Recently symbolic-numerical methods based on a spectral/Galerkin approach was applied to obtain approximate nonlinear planar and nonlinear orbital models for the rotor dynamics. Such models display quite good predictions of the studied rotordynamics (Moreira et al. [15]and [16]).

Following past work of Antunes et al. [1] in which the vibrations and stability of asymmetrically-supported rotors were studied, we present here an analysis of the linear and nonlinear rotor-dynamics, as a function of the support stiffness-asymmetry and of the rotor eccentricity. Theoretical stability domains are computed from the eigenvalues of the improved linearized model (Moreira et al. [14]). Finally, based on the symbolic-numerical method recently presented (Moreira et al. [16]), we display time-domain numerical simulations of stable solutions and nonlinear limit-cycles which stem from linearly-unstable solutions.

2 Flow formulation

Consider the geometry of the fluid annulus represented in Figure 1, where θ and t are respectively the azimuth and time, R is the rotor radius, $u(\theta,t)$ is the gap-averaged tangential flow velocity and $h(\theta,t)$ is the annular gap depth.

As in [2] the following simplifying assumptions will be adopted concerning the flow field: (i) The flow is modeled as being two-dimensional and incompressible; (ii) The radial gradients in the velocity and pressure fields are neglected; (iii) The dissipative effects due to turbulent shear stresses at the walls are modeled using semiempirical loss-of-head terms.

Given the above assumptions one can obtain the continuity equation for incompressible flow and the momentum equation (projected in the tangential direction),

$$\frac{\partial h}{\partial t}+\frac{1}{R}\frac{\partial (hu)}{\partial \theta}=0,\ \rho\left\{\frac{\partial (hu)}{\partial t}+\frac{1}{R}\frac{\partial \left(hu^2\right)}{\partial \theta}\right\}+\tau_s+\tau_r+\frac{h}{R}\frac{\partial p}{\partial \theta}=0, \qquad (1,\,2)$$

where ρ is the fluid density and $p(\theta,t)$ is the gap-averaged pressure.

The shear stresses at the rotor and stator walls, in equation (2), are given by

$$\tau_s(\theta,t)=\frac{1}{2}\rho u|u|\,f_s,\ \tau_r(\theta,t)=-\frac{1}{2}\rho(\Omega R-u)|\Omega R-u|\,f_r, \qquad (3,\,4)$$

where f_r and f_s are empirical friction coefficients, which depend on the flow Reynolds number and on wall roughness. Assuming $f_r=f_s=f$ and adopting the simplifications discussed in [3], we can deduce $\tau_s+\tau_r\simeq\rho f\Omega Ru-\frac{1}{2}\rho f\Omega^2R^2$.

Two main directions can be followed to obtain rotordynamic models from this approach.

Linearized flow equations/coupled system The first one, completely described in Moreira et al. [14], uses classical perturbation analysis and leads to linearized model for the flow forces. Introducing the structural dynamic forces one can study the modal behavior of the coupled system as a function of ε and Ω, by solving the complex eigenvalue $\lambda_n=\sigma_n+i\nu_n$ and complex eigenvector $\{\Phi_n\}$ problem of the set of five first order differential equations:

$$\mathbf{N}_1\dot{V}+\mathbf{N}_2V=\bar{0} \qquad (5)$$

where $V=(X,Y,Z,W,C)^T$, $Z=\dot{X}$, $W=\dot{Y}$ and C represents the first order fluctuating term of the average tangential flow velocity. From each eigenvalue $\lambda_n=\sigma_n+i\nu_n$ the corresponding modal frequency (in Hz) and modal damping can be defined as $\frac{\nu_n}{2\pi}$ and $-\sigma_n$. Note that 0, 1 or 2 complex conjugate pairs of eigenvalues (and eigenvectors) would be expected in the complete set of five eigenvalues (and eigenvectors) of the problem. One of these eigenvalues must be always real. Note that the coupling matrices depend on Ω and ε but are otherwise constant. One can find a detailed description of this approach in Moreira et al. [14].

Nonlinear flow equations/coupled system Using complex analysis techniques equations (1) and (2) can be exactly solved in order to deduce nonlinear version of the flow forces as functions of the parameters Ω, X and Y. Introduction the structural dynamic forces one obtain the nonlinear motion equations of the rotor-flow coupled system. Observe that, as in the linear case, the dynamics of the system depends not only on $X(t)$ and $Y(t)$ but also on a new variable called $C^{\mathrm{nl}}(t)$ which represent here a quantity proportional to the average tangential flow velocity. This approach is completely described in Moreira et al. [12].

Alternatively, a symbolic-numerical formulation, using a spectral/ Galerkin approximation of the flow velocity and pressure fields can be adopted to obtain a satisfactory rotordynamic model. Following this approach, the gap-averaged tangential flow velocity $u(t,\theta)$ and the gap-averaged pressure $p(t,\theta)$ are approximated, in the equations (1) and (2), by truncated Fourier series with time-dependent coefficients. The Galerkin method (see, for instance, Zwillinger [22] and Reddy [21]) applied over the residuals so obtained, generate a set of simultaneous ordinary differential-algebraic equations for the time-dependent coefficients. Finally, the set of differential-algebraic equations deduced is solved numerically in parallel with the dynamics equations for the structure yielding an approximate solution for the motions $X(t)$ and $Y(t)$. This set constitute, with the equations for the rotor-flow coupled system, the approximate rotor dynamics model, called $N\times M$ model. Note that the rotordynamics $N\times M$ model developed using this methodology constitute a set of differential-algebraic equations (DAE's). This class of problems arise naturally in many applications but present numerical and analytical difficulties which do not occur with systems of ordinary differential equations (see for instance Brenen et al. [4])

L (Rotor length [m])	0.250	Mass ratio, M_a/M^{st}	1.5
R (Rotor radius [m])	0.044	Reference struct. stiff., K^{st}_{ref} ($\frac{N/m}{10^4}$)	1.6
H (Annular gap [m])	0.0062	Damping in water (%)	0.5
$\delta = \frac{H}{R}$(Reduced gap)	0.14	Friction coef., $f = f_r = f_s$	0.01

Table 1: Main geometric, physical and modal parameters.

The accuracy of such approximate model depends, respectively, on the number N and M of terms used on the truncated Fourier series of $u(t,\theta)$ and $p(t,\theta)$. However, numerical results showed a quite good agreement between exact solutions and their low-order Galerkin approximations, see Moreira et al. [15] and [16]. This approach is exposed in these references and is the one we choose to use here in all the performed nonlinear numerical simulations.

3 Numerical simulations and discussion of results

In the following, and using the tools described in section 2, namely the linear model and the symbolic-numerical formulation, using a spectral/Galerkin approach, we present an analysis of the linear rotordynamics and some nonlinear simulations.

To do so, theoretical stability domains were computed from the eigenvalues of the linearized model and stability charts were built. Such stability charts were defined as a function of the spinning velocity and the asymmetry-ratio $\beta = \frac{K^{st}_X}{K^{st}_Y}$ (where K^{st}_X and K^{st}_Y stand for the structural stiffinesses) and of the rotor reduced eccentricity $\epsilon = \frac{X_0}{H}$ (where X_0 is the structural static eccentricity and H is the average gap). That is, we computed stability charts rpm$\times\beta$ (or rpm$\times 1/\beta$) and rpm$\times\epsilon$. In these charts, the white color represent the region of predicted linear stability. A grey scale translate the instability domain which is qualitatively characterized by the different types of instabilities predicted by the linear model. The qualitatively different types of instabilities are described by vertical grey bars near each figure: one can find the occurrence of divergence or flutter associated with the different rotordynamic modes (zero frequency/ backward whirl/ forward whirl modes). Note that the stiffness-asymmetry β is defined here as $\beta = \frac{K^{st}_X}{K^{st}_Y}$. This mean that $0 < \beta < \infty$ theoretically. However, in presenting our results, the stability charts were computed for $0 < \beta \leq 1$ whenever $K^{st}_X \leq K^{st}_Y$ using $K^{st}_X = K^{st}_{ref}$ and $0 < 1/\beta \leq 1$ if $K^{st}_Y \leq K^{st}_X$ using $K^{st}_Y = K^{st}_{ref}$. Note that whenever $\epsilon \neq 0$, because the reduced eccentricity is defined and implemented (along the direction X) as $\epsilon = \frac{X_0}{H}$, the stability charts for $0 < \beta \leq 1$ and $0 < 1/\beta \leq 1$ are not similar.

Campbell diagrams to illustrate the modal behavior of some chosen configurations are also presented. Note that the modal curves show and additional zero frequency mode, discussed in Moreira et al. [14]. In those diagrams, zero frequency modes are represented by a thin line, the backward whirl mode by a thick size line and the forward whirl mode by a medium size line.

Finally, we present time-domain numerical simulations of some stable solutions and nonlinear limit-cycles which stem from linearly-unstable solutions.

The main geometric, physical and modal parameters used on numerical simulations can be consulted in Table 1.

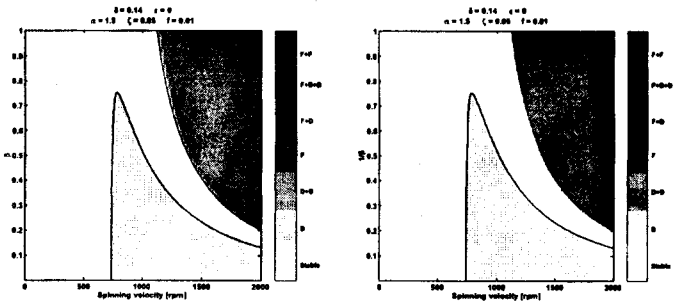

Figure 2: Stability charts rpm$\times\beta$ and rpm$\times 1/\beta$ for $\epsilon = 0$.

In Figure 2 the stability charts rpm$\times\beta$ and rpm$\times 1/\beta$ for an eccentricity $\epsilon = 0$ are presented. Note that in this case ($\epsilon = 0$) these charts must be similar. Observe that, interestingly, the stability range increases as β decrease for $0.75 \leq \beta \leq 1$. For this range one can find the occurrence of a flutter type instability at each corresponding regime. When $\beta = 0.75$ one verifies that the range of stability abruptly decreases and for $\beta \leq 0.75$ one can now observe the occurrence of a divergence type instability at about 750 rpm and later the occurrence of a flutter type instability after a restabilization range. Note that for $\beta \leq 0.75$ (and for centered rotors) this parameter (the stiffness-asymmetry) seems not to have influence on the rotordynamic stability range.

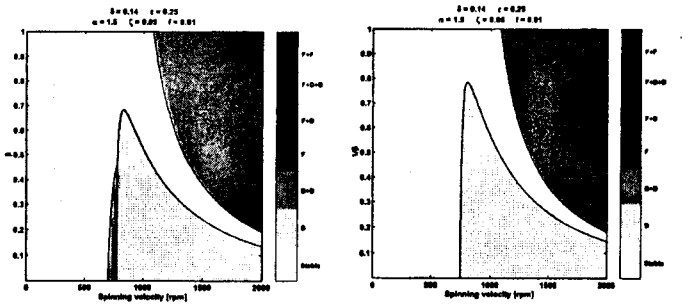

Figure 3: Stability charts rpm$\times\beta$ and rpm$\times 1/\beta$ for $\epsilon = 0.25$.

In Figures 3—5, for reduced eccentricities $\epsilon = 0$, $\epsilon = 0.25$ and $\epsilon = 0.75$, we display the corresponding rpm$\times\beta$ and rpm$\times 1/\beta$ stability charts. Observe that as the reduced eccentricity increases, the differences between rpm$\times\beta$ and rpm$\times 1/\beta$ stability charts get more and more significant showing that the rotordynamic stability depend on the directions along which the eccentricity and/or the stiffness asymmetry are applied . Clearly, for large reduced eccentricities ($\epsilon = 0.75$) one can find larger stability ranges for $0 < 1/\beta \leq 1$ (that is, assuming $K^{st}_X > K^{st}_Y$) than for $0 < \beta \leq 1$ (that is, assuming $K^{st}_Y > K^{st}_X$). This fact suggest that for a given reduced eccentricity it is possible to improve the stability range by implementing an appropriate asymmetry-ratio. One can conclude that for asymmetrically supported rotors the stability range decreases if eccentricity is applied along the axis of the lower support stiffness value.

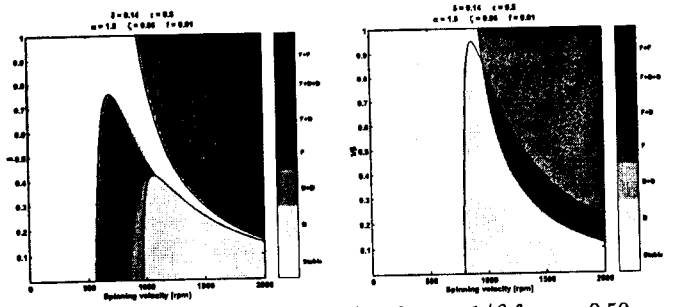

Figure 4: Stability charts rpm×β and rpm×$1/\beta$ for $\varepsilon = 0.50$.

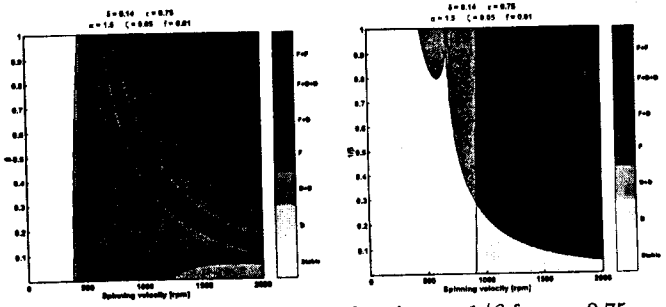

Figure 5: Stability charts rpm×β and rpm×$1/\beta$ for $\varepsilon = 0.75$.

From Figures 2—5 one can also confirm (observing the line $\beta = 1/\beta = 1$) that for symmetrically supported rotors the stability range always decreases when the eccentricity increases.

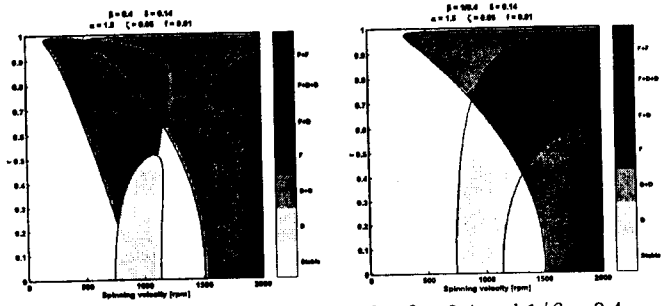

Figure 6: Stability charts rpm×ε for $\beta = 0.4$ and $1/\beta = 0.4$.

Finally, in Figure 6, stability charts rpm×ε for $\beta = 0.4$ and $1/\beta = 0.4$ are displayed. One observe that typically in both charts a maximum stability range is verified for about $\varepsilon \approx 0.2$ (chart for $\beta = 0.4$) and $\varepsilon \approx 0.7$ (chart for $1/\beta = 0.4$), respectively. This fact tends to confirm that it is possible to improve the stability range choosing appropriate eccentricities/stiffness asymmetry-ratios. Note that for large eccentricities Figure 6 must be interpreted with some reserve. Indeed for these range of eccentricities the linearizing assumptions are not verified.

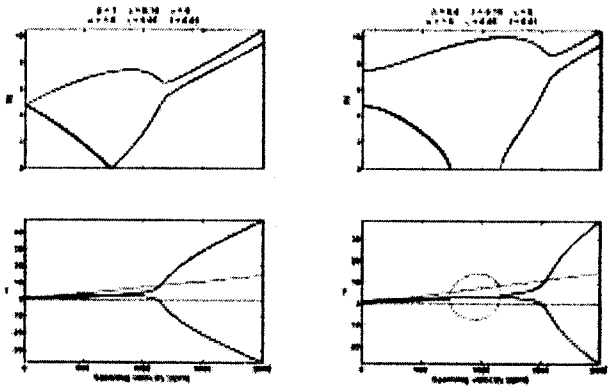

Figure 7: Campbell diagrams for $\beta = 1.0$ and $\beta = 0.4$ ($\varepsilon = 0$).

In Figure 7 we present Campbell diagrams for chosen configurations. In those diagrams one can observe the predicted modal frequencies and damping as a function of the spinning velocity.

In Figure 7, and for a reduced eccentricity of $\varepsilon = 0$, we display the Campbell diagrams for $\beta = 1$ and $\beta = 0.4$. One observe that for $\beta = 1$ our system is unstable (by flutter in the forward whirl mode) above the spinning velocity at about 1100 rpm. For $\beta = 0.4$ our system become unstable by divergence between 750 and 1200 rpm. The predicted restabilization regimes between 1200 and 1500 rpm can be observed in this system. The described dynamics can be also deduced by observing Figure 2. Note the agreement between the information reported by the Campbell diagrams and the stability charts.

Finally, in Figures 8—10, time-domain numerical simulations (representing 10 seconds of free response) of stable solutions and nonlinear limit-cycles which stem from linearly-unstable solutions are displayed.

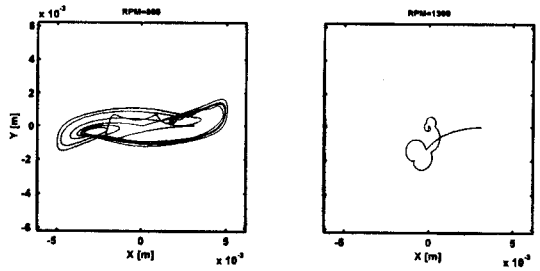

Figure 8: Nonlinear simulations: $\beta = 0.4$ and $\varepsilon = 0$.

In Figure 8 we observe a backward whirling high amplitude limit-cycle at 800 rpm. Note that linear theory predicts instability by divergence between 700 and 1150 rpm (see Figure 7, right). Interestingly, one verifies the occurrence of a restabilization, between 1150 and 1500 rpm, observing the stable behavior at the spinning velocity of 1300 rpm. This phenomenon is also predicted by linear theory.

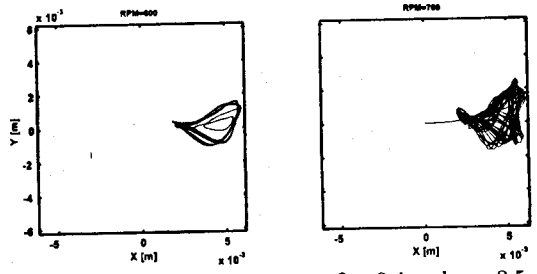

Figure 9: Nonlinear simulations: $\beta = 0.4$ and $\varepsilon = 0.5$.

In Figures 9-10 we compare, for and eccentricity $\varepsilon = 0.5$, the behavior of our system when the asymmetry stiffness-ratios are $\beta = 0.4$ and $1/\beta = 0.4$. We constat that for $\beta = 0.4$ (Figure 9) our system display backward whirling high amplitude limit-cycles which stem from linearly-unstable solutions for both regimes (600 and 700 rpm). Note that the linear theory predicts a larger stability range for $1/\beta = 0.4$ (see Figure 4). Indeed, for $1/\beta = 0.4$ (Figure 10) our system does not display a linearly-unstable solution at the spinning velocity of 600 rpm, confirming the existence of the referred larger stability range. However, this configuration ($1/\beta = 0.4$), for a spinning velocity of 700 rpm display a backward whirling high amplitude limit-cycle stemming from a linearly-unstable solution which is not predicted by the corresponding stability chart in Figure 4. This fact is not a surprise if we remember that the stability charts do not account for the influence of the rotor drift which increases the actual eccentricity and is naturally accounted for by nonlinear numerical simulations.

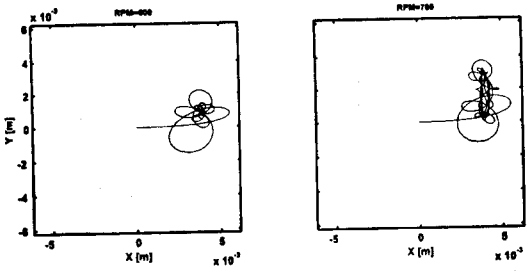

Figure 10: Nonlinear simulations: $1/\beta = 0.4$ and $\varepsilon = 0.5$.

4 Conclusions

In this paper, we briefly summarize the theoretical approaches used in the numerical simulations and present an analysis of the linear rotor-dynamics, as a function of the support stiffness-asymmetry and of the rotor eccentricity. Theoretical stability domains are computed from the eigenvalues of the linearized model enabling us to built theoretical and complete stability charts. Finally, we present time-domain numerical simulations of stable solutions and nonlinear limit-cycles which stem from some linearly-unstable solutions.

Concerning the effects of the support asymmetry β and reduced eccentricity ε one can conclude: (i) For centered rotors the stability range increase as β decrease (that is, increasing the stiffness asymmetry) for $\beta_{\text{lim}} \leq \beta \leq 1$, where β_{lim} depend on the rotor configuration. For $0 < \beta < \beta_{\text{lim}}$ this parameter does not have significant influence on the stability range. (ii) For symmetrically supported rotors configuration the stability range always decreases when the eccentricity increases. (iii) For asymmetrically supported rotors the stability range decreases if eccentricity is applied along the axis of the lower support stiffness value. Conversely the stability range increases when eccentricity is applied along the axis of the upper stiffness value.

These results may be of industrial relevance and confirm that it is possible to improve the stability range choosing appropriate eccentricities/stiffness asymmetry-ratios. We note that this fact was stressed before by Antunes et al. [1].

Despite using recently developed theoretical tools, the reported linearized predictions do not account for the rotor drift (and so the dynamic eccentricity) which strongly govern the system dynamics.

Experimental work is currently being done to further assess the validity of the reported theoretical results.

5 Acknowledgments

This project has been endorsed by the Portuguese FCT and POCTI, with funding participation through the EC programma FEDER.

References

[1] Antunes, J., Grunenwald, T., Axisa, F. & Bennet, G. Vibrations and stability of asymmetrically supported rotors with annular fluid confinement. *Proc. of the Int. Conf. on Structural Dynamics, Vibration*, Noise and Control, Hong Kong, December 5-7, 1995.

[2] Antunes, J., Axisa, F & Grunenwald, T. Dynamics of Rotors Immersed in Eccentric Annular Flow: Part 1 - Theory. *Journal of Fluids and Structures* **10**, pp. 893-918, 1996.

[3] Antunes, J., Mendes, J., Moreira, M & Gunenwald, T. A Theoretical Model for Nonlinear Planar Motions of Rotors under Fluid Confinement. *Journal of Fluids and Structures* **13**, pp. 103-126, 1999.

[4] Brenan, K. E., Campbell, S. L. and Pezold, L. R. Numerical Solution of Initial-Value Problems in Differential-Algebraic Equations. SIAM, 1996.

[5] Axisa, F. & Antunes, J. Flexural Vibrations of Rotors Immersed in Dense Fluids: Part 1—Theory. *Journal of Fluids and Structures*, **6**, pp. 3-21, 1992.

[6] Black, H. Effects of Hydraulic Forces in Annular Pressure Seals on the Vibrations of Centrifugal Pump Rotors. *I. Mech. E. Journal of Mechanical Engineering Science* **11**, pp. 206-213, 1969.

[7] Childs, D. Finite length solutions for rotordynamic coefficients of turbulent annular seals. *ASME Journal of Lubrification Technology*, **105**, pp. 437-444, 1983.

[8] Fritz, R. The Effects of an Annular Fluid on the Vibrations of a Long Rotor: Part 1—Theory. *ASME Journal of Basic Engineering*, **92**, pp. 923-929, 1970.

[9] Grunenwald, T., Axisa, F. & Antunes, J. Rotor Vibration under Fluid Confinement: Analysis of Dissipative Phenomena and Stability. *Journal of Fluid and Structures*, **10**, pp. 919-944, 1991.

[10] Grunenwald, T. *Comportement Vibratoire d'Arbres de Machines Tournantes dans un Espace Annulaire de Fluide de Confinement Modéré.* Doctoral Thesis, Paris University, 1994.

[11] Hirs, G. G. A Bulk-Flow Theory for Turbulence in Lubricant Films. *ASME Journal of Lubrication Technology*, **95**, pp. 137-146, 1973.

[12] Moreira, M., Antunes, J. & Pina H. A Theoretical model for nonlinear orbital motions of rotors under fluid confinement. *Journal of Fluid and Structures* **14**, pp. 635-668, 2000.

[13] Moreira, M., Tissot, A. & Antunes, J. Experimental Validation of Theoretical Models for the Linear and Nonlinear Vibrations of Immersed Rotors. *Proc. of the 8^{th} International Symposium on Transport Phenomena and Dynamic of Rotating Machinery*, ISROMAC-8 (Honolulu, Hawai, USA), II, March 2000, pp. 857-865, 2000.

[14] Moreira, M, Antunes, J. & Pina, H. An Improved Linear Model for Rotors Subjected to Dissipative Annular Flows. *Proc. of the 7^{th} International Conference on Flow-Induced Vibration*, FIV2000 (Lucerne, Switzerland), June 19-22, 2000, eds. S. Ziada & T. Staubli, A.A. Balkema: Roterdam pp. 767-776, 2000.

[15] Moreira, M., Antunes, J. & Pina H. A symbolic-numerical method for nonlinear rotordynamics under fluid confinement, *Proc. of the 2000 ASME Int. Mech. Eng. Cong. and Expo*, IMECE 2000 (Orlando, Florida, USA), DE-Vol. **108**/DSC-Vol. **68**, pp. 61-68, 2000.

[16] Moreira, M., Antunes, J. & Pina H. Analysis of the nonlinear orbital motions of immersed rotors using a spectral/Galerkin approach, Accepted for presentation in the 8^{th} Int. Congress on Sound & Vibration, ICSV8 (Hong Kong, China), July 2-6, 2001.

[17] Nelson, C. Rotordynamic coefficients for compressible flows in tapered annular seals. *ASME Journal of Tribology*, **107**, pp. 318-325, 1985.

[18] Nordmann, R., Dietzen, F. & Weiser, H. Calculation of rotordynamic coefficients and leakage for annular gas seals by means of finite difference techniques. *ASME Journal of Tribology*, **111**, 545-522, 1989.

[19] Ramsden, J., Ritchie, G. & Gupta, J. The Vibrational Response Characteristics of a Design for the Sodium Pumps of the Commercial Fast Reactor. *Proc. I. Mech. E. Fluid Machinery and Nuclear Energy Groups Convention: Pumps For Nuclear Power Plant.* Bath, April 1974, Paper C107/74, 187-pp. 196, 1974.

[20] Ramsden, J., Jones, H. & Cowking, E. Vibration of the P.F.R. Primary Sodium Pumps. *Vibrations and Noise in Pump, Fans and Compressor Installations.* Southampton, September 1975, Paper C103/75, pp. 21-33, 1975.

[21] Reddy, J. N. *Applied Functional Analysis and Variational Methods in Engineering.* McGraw-Hill, 1986.

[22] Zwillinger, D. *Handbook of Differential Equations.* Academic Press, 1997.

Section 3:
Vibration analysis and control